Identification and Visualization of the Full-Ring Deformation Characteristics of a Large Stormwater Sewage and Storage Tunnel Using Terrestrial Laser Scanning Technology

Zixin Zhang [1,2], Tong Yin [1,2], Xin Huang [1,2,*], Fan Zhang [3], Yeting Zhu [4] and Wei Liu [1,2]

[1] Department of Geotechnical Engineering, College of Civil Engineering, Tongji University, Shanghai 200092, China; zxzhang@tongji.edu.cn (Z.Z.); yintong@tongji.edu.cn (T.Y.); 1510248@tongji.edu.cn (W.L.)
[2] Key Laboratory of Geotechnical and Underground Engineering, Ministry of Education, Tongji University, Shanghai 200092, China
[3] Shanghai Urban Construction Design & Research Institute, 3447 Dongfang Road, Shanghai 200125, China; zhangfan1@sucdri.com
[4] Shanghai Tunnel Engineering Co. Ltd., Shanghai 200082, China; 1210278theronzhu@tongji.edu.cn
* Correspondence: xhuang@tongji.edu.cn

Abstract: Constructing deeply-buried stormwater sewage and storage tunnels is an effective method to mitigate the waterlogging and sewer overflow problems in modern cities. Prior to construction of such tunnels, a structural loading test is essential for acquiring the mechanical responses under complex loading conditions, such as cyclic inner hydraulic head, during which capturing the full-ring deformation of the tunnel lining is significant for a comprehensive understanding of the tunnel's mechanical behaviors. This paper introduces the application of terrestrial laser scanning (TLS) technology in the full-scale structural loading tests of a large stormwater sewage and storage tunnel, which gives the full-ring deformation throughout the tests. A data processing methodology was developed to extract the key data points of the lining segments from the original data cloud by removing noise points and mitigating data jump, based on which the deformation of testing the lining segments at arbitrary locations can be calculated. Furthermore, a post-processing software was developed to visualize the full-ring deformation. The full-ring deformation at different loading conditions and its evolution under cyclic loading were captured. It is shown that the lining's convergence deformation is more sensitive to the inner hydraulic head than to the external soil-water pressure, and the deformation cannot fully recover in a water-inflow-and-drainage cycle due to the presence of joints.

Keywords: terrestrial laser scanning; full-scale loading tests; stormwater sewage; storage tunnel; data processing; deformation visualization

1. Introduction

Modern cities nowadays encounter serious issues related to waterlogging and sewer overflow due to population expansion and aging of drainage systems, especially in the rainy seasons. Seeking new approaches to control the waterflow in cities during the heavy rainfalls is urgent to mitigate this problem. Building large stormwater sewage and storage tunnels might be a viable way, through which the existing drainage systems are integrated with the deeply buried tunnels, whose downstream sides are connected to wastewater treatment plants. When the rainfalls exceed the processing capacity of the city's drainage systems, the stormwater will be collected and transported into the tunnels.

After treatment, the stormwater will be discharged to rivers or reservoirs. A common practice to construct such tunnels is to use a TBM (tunnel boring machine) due to its advantages of little disturbance to the surrounding ground and good safety and settlement control.

Compared to normal tunnels, the stormwater sewage and storage tunnel may experience large and repeating inner water pressure apart from the ordinary external soil-water pressure, which might induce special mechanical behaviors. Therefore, prior to construction, it is important to acquire the structural behaviors of the segmental tunnel lining. The full-scale structural loading test is regularly used to investigate the mechanical response, i.e., internal forces and deformation, of the tunnel lining [1–3]. Particularly, the development and evolution of convergence deformation need to be recorded throughout the tests as it is one of the key factors reflecting the performance and durability of the segmental tunnel lining, which could provide valuable insight for engineering practice.

Traditionally, the tunnel lining deformation during a loading test can be measured either through a total station or using a cable displacement transducer, which is also known as 'single point measurement'. However, a total station or a cable displacement transducer only delivers a set of data at selected disperse points. Neither of them can give a full picture of how the segment deforms as a whole [4]. Therefore, the deformation characteristics at some key sections may be lost. Digital photogrammetry is another widely applied technique, but it requires sufficient lighting conditions and distinct texture on the surface of the measured object [5,6], which may not be fully guaranteed during the test. Due to the shortcomings of above methods, the terrestrial laser scanning (TLS) technique has gained increasing attention in geotechnical engineering in recent years, as it is a non-contacting and non-destructive measurement technique which is fast and accurate [7]. TLS is an image recording and processing technology using scanners that transmit and collect laser pulses reflected from physical objects, and storing the locations of millions of points in space wherever the scanner can reach [8]. In this way, the full-ring deformation data, rather than deformation data at disperse locations, can be obtained by analyzing the collection of data points, which is termed as 'point cloud data'. The applications of TLS have been widespread in many fields, especially in geometry documentation and structure monitoring of, e.g., landforms [9–11], building structures [12–14], road markings [15–17], river banks [18–20], pipelines [21,22], landslides [23–25], and tunnels [26–30].

The size of point cloud data could be significantly large due to the high resolution of TLS technology and the noise points of unnecessary objects around the site. Consequently, it is important to develop a method that could automatically and efficiently process the point cloud data and visualize them in a desired way. Recent efforts have been devoted to improving the efficiency and practicability of data processing for the point cloud data in tunneling projects. Basically, two methods are frequently used to extract the tunnel cross-section from point cloud data [31]. The first method refers to the mesh modeling technique, which approximates the geometry of a tunnel cross-section through generation of a full 3D mesh model. This method can capture the detailed 3D features of the tunnel lining, but bears the risk of adding an additional level of errors as it is a secondary interpolation of TLS data [31]. Furthermore, this method is computationally uneconomic. Tsakiri et al. [32] introduced the mesh modeling technique for deformation monitoring in a beam loading test, which inspired the applications of this method in tunnel deformation measurement. Gikas [31] discussed the application of the mesh modeling technique in processing TLS data, and suggested that with proper mesh models and sufficient computational resources, the three-dimensional tunnel profile could be precisely extracted. Fekete et al. [8] successfully extracted the 3D tunnel profile of a drill-and-blasting tunnel using the mesh modeling technique. They showed that a TLS system made it possible to remotely acquire the detailed configuration of the excavated rock mass during tunnel construction. The application of this method could also be found in [4,33]. The second method employs a 'plane projection' strategy, which only considers a data volume subset of the point cloud. By projecting the points onto a pre-defined plane, a thin and sliced tunnel cross-section can be obtained through certain curve fitting algorithms. Compared to the mesh modeling technique, this method is easier to implement and enables faster calculation. However, the 3D features of the tunnel lining would be lost due to the projection process,

and the accuracy of extraction depends largely on the curve fitting algorithm. Yoon et al. [34] used this method for tunnel profile extraction and damage detection. With the development of laser scanning hardwares, 'plane projection' has been used more frequently over the recent years. Han et al. [35] presented this method for extracting the tunnel cross-sections. By projecting the three-dimensional point cloud data onto a two-dimensional plane, the tunnel cross-section was reflected by planar images, through which tunnel deformation was precisely obtained. Cheng et al. [36] adopted the projection strategy to extract tunnel cross-sections from in-site scanned data and proposed a filtering algorithm to remove non-lining points. Walton et al. [37] developed an elliptical fitting algorithm to improve the change detection capabilities for tunnel deformation monitoring, which could analyze the time-dependent behavior of tunnel deformation. More application case histories of this method can be found in [38–41].

Though the methods mentioned above have shown satisfactory performance in practice, the application of TLS technology in measuring tunnel deformation is still challenging due to the existence of joints and hand holes, which create discontinuities in the curvature and brings about many points of noise in the data cloud. These issues have not been resolved satisfactorily in both scientific and commercial works. Furthermore, the applications of TLS technique in loading tests on tunnel lining have yet been addressed. This paper proposes an automatic data processing and visualization method, which could process the point cloud data of tunnels in the loading tests. Compared with the existing methods mentioned above, this method could deal with tunnels of different cross-section shapes. The structure of the paper is as follows: firstly, the fundamental principles and workflow of applying TLS to measure the full-ring deformation of lining structure are introduced; the methodology of extracting the contour of tunnel cross-section from the three-dimensional point cloud data is elucidated; then a post-processing software called 'Cloud Viewer' is developed to visualize the tunnel deformation; finally, the validity and effectiveness of the proposed method are demonstrated through an application example investigating the mechanical response of a stormwater sewage and storage tunnel.

2. Methodology of TLS Technology

2.1. Principles and Workflow of TLS in Tunnel Loading Tests

TLS technology originates from pulse ranging method, which is widely used for distance measurement [42,43]. In the pulse ranging method, the laser transmitter emits laser beams to the measuring points. After diffuse reflection by the surface of the scanned object, the reflected laser beams are collected by the laser receiver. The distance between the measuring point and the laser scanning station is calculated by the difference between the time of emitting and receiving the laser beams [31]. When the distance is obtained by the pulse ranging method, the coordinates of the measuring points could be acquired by simple transformation equations [40].

The spatial properties of millions of points are recorded to depict the scanned object, through which precise information regarding the three-dimensional geometric features can be provided with a high sampling density [34]. The workflow of applying TLS technology in loading tests on segmental lining is shown in Figure 1, in which three major procedures are classified as (1) laser scanning; (2) data processing; and (3) post-processing. The laser scanning process would be introduced briefly in this section, while the data processing and post processing would be elucidated in details in Sections 2.2 and 2.3, respectively.
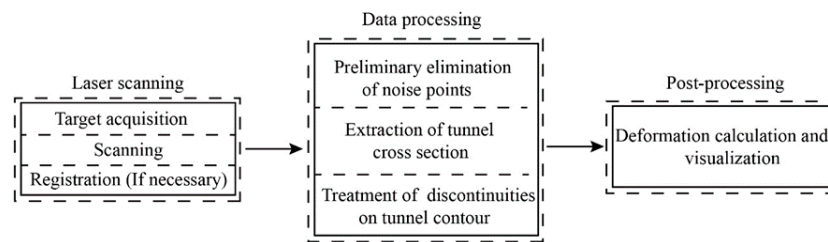
Figure 1. Workflow of the application of TLS on tunnel lining loading test.

Before object scanning, a 'target acquisition' [33] procedure needs to be conducted, in which the global coordinate system is established by locating several targets attached on the stationary spots such as walls and ground. The spatial properties of the central points of the targets would be firstly measured and identified in the point cloud data. Then, coordinates of the points on the scanning objects could be obtained in the coordinate system determined by these targets. Figure 2 presents a sample target used on site and the corresponding point cloud image. It should be noted that, occasionally, obstructions exist in front of the laser scanning station in the loading test, creating a certain area of a 'blind zone' that is referred to as occlusion where the laser beams cannot reach. Therefore, multiple laser scanning stations at different locations may be used in such cases to obtain a complete point cloud data of the tunnel segmental lining. The point cloud data of different stations could be merged via an operation called 'registration' [40]. 'Registration' is based on the fact that as the scanning stations identify the same targets, and that a universal global coordinate system can be established and shared by the point cloud data from different stations. This step is conducted within the commercial software, Leica Cyclone [44], which provides a powerful tool to facilitate the registration process.
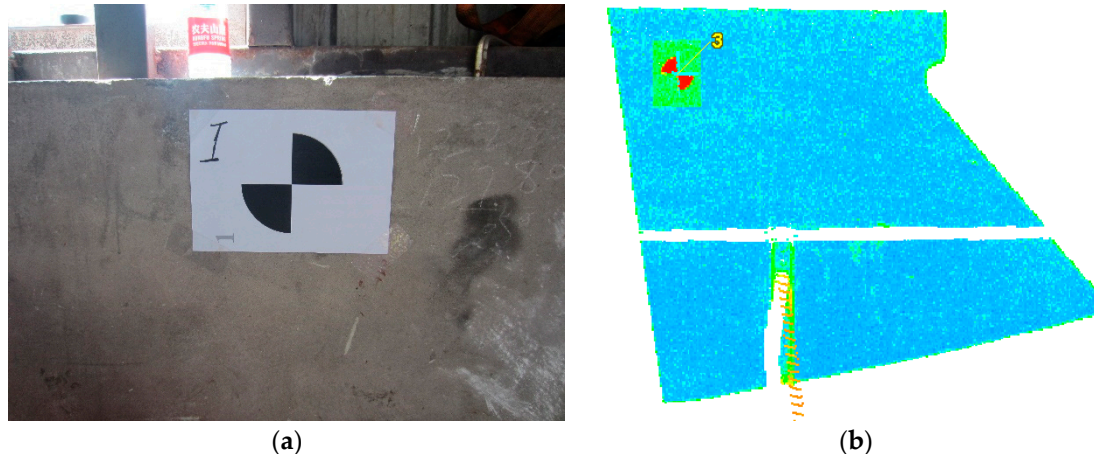

(**a**)   (**b**)

Figure 2. Sample targets used for establishing the global coordinate system: (**a**) picture of a target used on site; and (**b**) an image of the point cloud of targets.

2.2. Major Procedures of Data Processing

The proposed data processing methodology shown in Figure 2 consists of three major procedures: (1) preliminary elimination of noise points; (2) extraction of the tunnel cross-section; and (3) treatment of discontinuities of tunnel contours. Firstly, the raw point cloud data needs to be processed to gain the contour of tunnel lining. As many unnecessary objects may have also been scanned and included in the point cloud data, preliminary elimination is necessary to exclude these noise points from the raw data. Consequently, the contour of the tunnel cross-section could be extracted by the proposed method. Note that due to the existence of hand holes or other grooves on the segments, discontinuities would inevitably occur on the contour of the tunnel lining, which needs to be specially treated; otherwise data jump (unrealistic deformation values) would create unreliable results for the deformation analysis.

Finally, once a continuous contour of the deformed tunnel lining becomes available, the deformation data could be visualized via the software 'Cloud Viewer' with various display features that have been embedded.

2.2.1. Preliminary Elimination of Noise Points

Before extracting the tunnel cross-section, in order to obtain an optimal extraction accuracy, obvious noise points caused by in-site surrounding objects such as walls, steels frames and cables of sensors (see Figure 3) need to be excluded from the raw point cloud data. Unlike the laser scanning inside a real tunnel, in the full-ring tests structures made of the same materials (concrete) as tunnel lining, e.g., walls and ceilings, would be included in the point cloud. These structures are marked in colors similar to the tunnel lining in Leica Cyclone, which makes it difficult to automatically conduct filtration using the intensity filter. Consequently, this procedure is conducted manually using Leica Cyclone software as it provides efficient fence tools of data pre-processing. Those data points that were obviously outside the area of testing the lining segment are identified as noise points and will be eliminated from the data cloud.
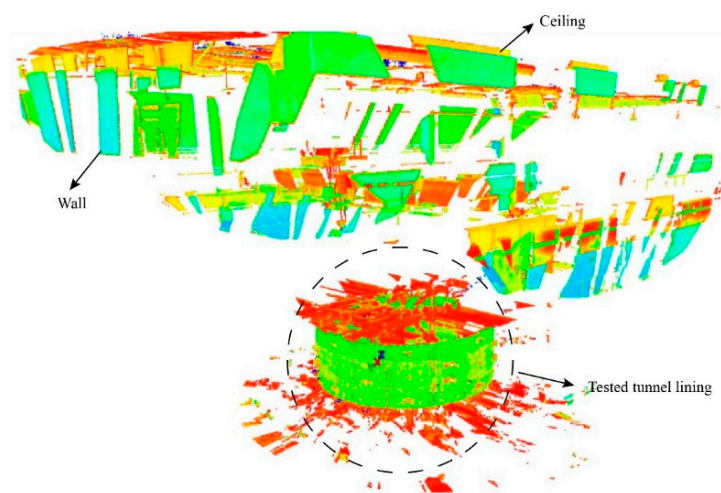

Figure 3. Raw laser scanning data of the site of a loading test on the tunnel lining.

After eliminating the obvious noise points, a rough three-dimensional contour of the tunnel lining could be acquired for further processing as shown in Figure 4.
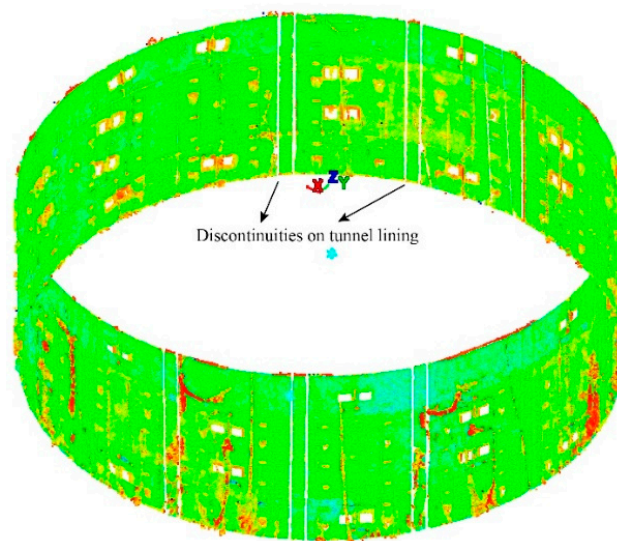
Figure 4. The pre-processed point cloud data of a sub-rectangular tunnel lining.

2.2.2. Extraction of the Tunnel Cross-Section

As discussed in Section 1, compared with the mesh modeling technique, the 'plane projection' method could extract the tunnel cross-section faster, and with a lower computational cost. The former is important as an instantaneous interpretation of convergence deformation of tested lining segments is desired to evaluate the structural status of tunnel lining at each loading stage. Thereby, the 'plane projection' method is adopted for deformation analysis in the current study.

In order to facilitate extracting the planar outline of the tunnel cross-section from the three-dimensional point cloud data, a polar coordinate system is firstly established with polar angles ranging from 1–360°. Then, the coordinates of points from the 'point cloud data are formalized following the simple transformation of coordinates from a Cartesian coordinate system to a polar coordinate system. This is commonly used in studies which adopt the 'plane projection' method to extract the tunnel cross-section, e.g., in [38,40].

Since the point cloud data could be extremely large with selected resolutions, thousands of points might exist at the same polar angle. Therefore, different lengths of radial vector ρ_i would occur at a polar angle $\theta = \theta_i$. In order to increase the processing efficiency, a statistical approach is employed, in which the occurrence of different values of ρ_i at $\theta = \theta_i$ is counted, and those points whose occurrence frequencies of ρ_i are smaller than half of the highest one would be excluded from the point cloud data, as these points might result from undeleted noise. The use of half of the highest occurrence frequency as the criterion to reduce the data points is flexible and depends on the scanning resolution. Then a representative value of radial vector length $\overline{\rho_i}$ is defined as:

$$\overline{\rho_i} = \frac{\sum\limits_{j=1}^{N} f_j \rho_i^{(j)}}{N} \tag{1}$$

where N and f_j are the number of remaining points and the occurrence of the radial vector length of $\rho_i^{(j)}$ on the remaining points at $\theta = \theta_i$, respectively.

After above operations, a 'representative point' $\overline{P_i}$ with representative values of θ_i and $\overline{\rho_i}$ is generated. By searching θ_i from 1° to 360°, the representative points along the outline of the tunnel lining could be obtained by an iteration process, creating a matrix containing a group of representative points.

In order to calculate the convergence deformation, a curve fitting algorithm has to be used for obtaining a continuous tunnel outline. Four fitting methods were commonly used in the literature,

namely planar least-square method, cylindrical fitting method, elliptical fitting method and RANSAC (random sample consensus) fitting method. Table 1 briefly summarizes the applications, advantages, and disadvantages of these methods. Note that it may be necessary to conduct full-scale loading tests for tunnels with an irregular cross-section, e.g., sub-rectangular tunnel [45]. In such cases, fitting methods with feasibility of processing arbitrary cross-section shapes are significant and necessary. Consequently, the least-squares method is selected for fitting the cross-section outline in the current study to standardize the data processing procedure. Once a continuous outline is obtained, the tunnel deformation at each point can be calculated by subtracting $\overline{\rho_i}$ on the extracted outline from that of the design outline.

Table 1. Summary of algorithms used for cross-section fitting.

Method	Applications	Advantages	Disadvantages
Planar least-square method	Yoon et al. [34]; Cheng et al. [36]	1. Easy implementation 2. Feasibility for arbitrary shapes of cross-section	Losing 3D features
Cylindrical fitting method	Xie and Lu. [40]	3D interpretation of 'point cloud'	Only feasible for circular tunnel
Elliptical fitting method	Walton et al. [37]; Tan et al. [39]	Easy implementation	Only feasible for circular tunnel
RANSAC fitting method	Kang et al. [38] Cao et al. [41]	Capability of smoothing data that contain a significant percentage of gross errors.	Complex in implementation

2.2.3. Treatment of Discontinuities on the Tunnel Contour

As there are some hand holes or grooves on the surface of the tunnel lining, after eliminating the obvious noise points in the preliminary elimination process, discontinuities may appear frequently on the outline of the tunnel lining as shown in Figure 4, which would induce 'data jump' of points at corresponding locations (see Figure 5). The deformations of adjacent points are supposed to be nearly continuous. Consequently, when an extremely large deformation value is captured and exceeds a pre-set limiting value (normally five times larger than the deformation of previous point), data jump is assumed to occur. The existence of data jump would impair the accuracy of the curve fitting.
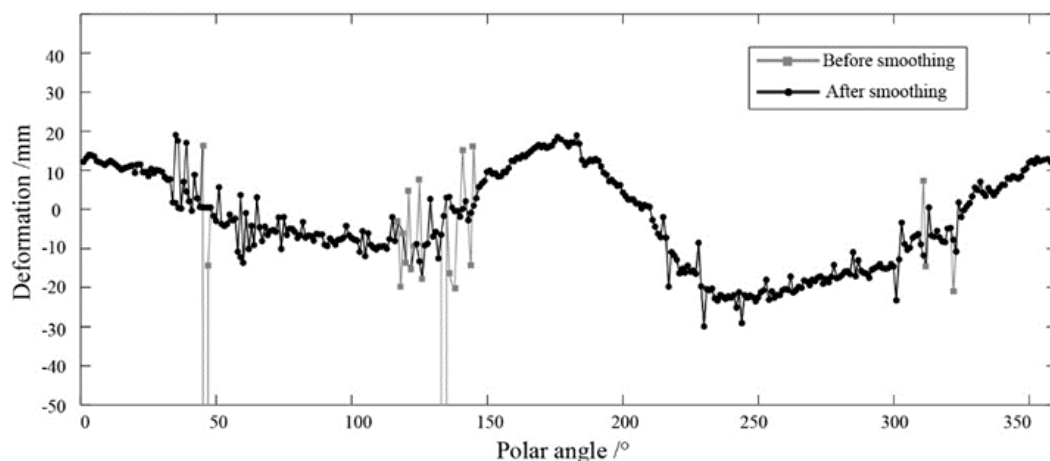

Figure 5. Comparison between the deformation distributions before and after smoothing.

To cope with data jump, a point regeneration scheme has been designed to smooth the tunnel outline, acquiring reasonable deformation values at the discontinuous spots. The principle of this treatment is based on the assumption that the deformations of adjacent points are approximately continuous, which indicates that the deformation difference between them would not be unreasonably large. The outline of the testing lining ring is angularly divided into 360 arcs, each of which has

a central angle of 1°. Hence, the point regeneration scheme firstly calculates the difference of the radial vector length (d_i) between every two adjacent points from 1° to 360°:

$$d_i = \overline{\rho_{i+1}} - \overline{\rho_i} \; (i = 1, 2, 3, \ldots, 360, d_{360} = \rho_1 - \rho_{360}) \tag{2}$$

This manipulation leads to a set $\overrightarrow{D} = \{d_1, d_2, \ldots, d_{360}\}$. Corresponding to the accuracy requirement, those elements in $\overrightarrow{D}$ whose absolute value is larger than the prescribed error limit χ, i.e., $|d_i| > \chi$, are selected elements that need to be smoothed, while those elements with $|d_i| \leq \chi$ are taken as the real points located at the tunnel periphery. For those elements that need to be smoothed and with successive subscripts, $d_m, d_{m+1}, \ldots, d_n$, if $\left| \sum_m^n d_i \right| < \chi$, an average value would be set as the values of these elements, i.e., $d_m = d_{m+1} = \ldots = d_n = \sum_{i=m}^n d_i / (m - n + 1)$. For instance, if $\chi = 10mm$, $d_1 = 90mm$, $d_2 = -120mm$, and $d_3 = 36mm$, one could obtain $|d_1 + d_2 + d_3| = 6mm < 10mm$, then we set $d_1 = d_2 = d_3 = 6mm/3 = 2mm$. Finally, the points on the discontinuous locations are regenerated as the difference between the lengths of radial vectors have been obtained by averaging, which completes the smoothing process. Figure 5 shows the comparison between the deformation distributions before and after smoothing, in which a distinct improvement regarding the continuity of deformation can be observed.
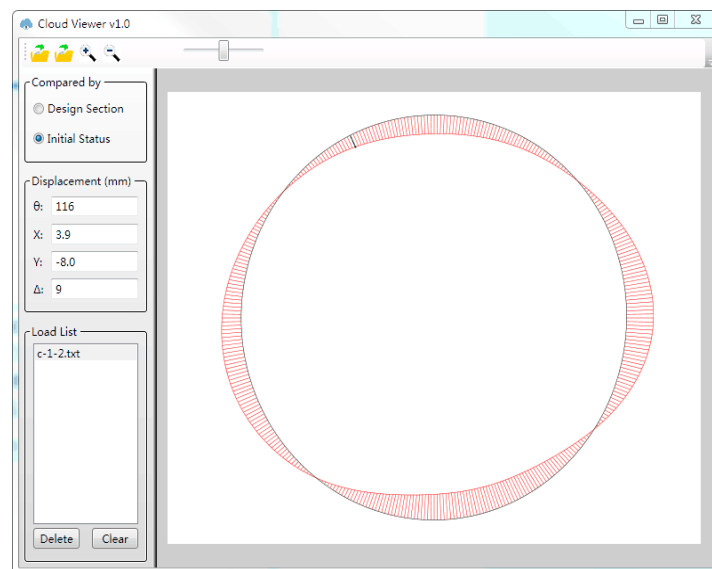
2.3. Deformation Visualization

In order to visualize the tunnel deformation clearly, an in-house post-processing software called 'Cloud Viewer' has been developed to convert the deformation data into graphical figures, on which the design and deformed tunnel outlines are depicted.

Figure 6a shows the graphical user interface (GUI) of 'Cloud Viewer', consisting of a panel for selecting the comparing cross-section, a panel for digitally displaying the displacement, a panel for selecting loading condition, a panel for graphically displaying deformation contour, and some functional buttons and tools. After the treated data of the tunnel outline have been imported, the user could choose to calculate the deformation either based on the designed cross-section or based on the initial status at the beginning of the loading test. Then, by inputting the polar angle of the desired point on the displacement display panel or clicking the corresponding position on the graphical deformation display panel, the x and y components and the resultant value of the deformation on points at arbitrary polar angles could be shown in the corresponding textbox. Since different loading conditions need to be considered in a tunnel lining loading test, the loading list panel facilitates the visualization of the deformation under different loading conditions at the same time. Considering that the scale of the deformation is much smaller than the tunnel diameter, it needs to be amplified to obtain a clear deformed contour of the tunnel lining. As shown in Figure 6, Cloud Viewer provides a convenient tool for setting an amplifying factor to visualize the tunnel deformation, which is achieved through multiplying the deformation by the assigned display factor.
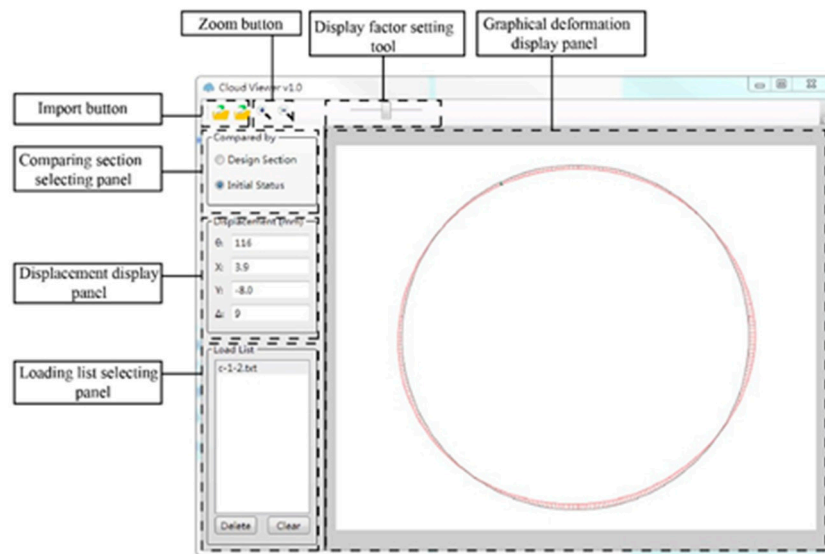
(**a**)

(**b**)

Figure 6. GUI of Cloud Viewer showing deformation visualized by multiplying different display factors: (**a**) display factor of 1.0; and (**b**) display factor of 4.

3. Project Background and Measurement Plan

The proposed method has been used to analyze the full-ring deformation during the loading test of a large stormwater sewage and storage tunnel under the Suzhou River in Shanghai. The validity of the method was verified by comparing the convergence deformation obtained using the laser scanning technology and that recorded by the cable displacement transducers at selected locations. This section introduces the details of the application of TLS in the structural loading test of this particular tunnel.

3.1. Project Background

The testing tunnel is a large stormwater sewage and storage tunnel, planned beneath the Suzhou River in Shanghai, China. It is the first time in Shanghai to construct such a large stormwater sewage and storage tunnel with a maximal burial depth up to 50 m and an internal hydraulic head (which refers to the height of water surface within the tunnel relative to the tunnel bottom) as large as 50 m, both of which will be unprecedented in Shanghai.

The tunnel has an inner diameter of 9 m and the lining ring is 650 mm in thickness. A single lining ring is 1.5 m in width and consists of eight segments radially fabricated by straight bolts. Furthermore, a special feature of such a tunnel is that it bears cyclic loads during service time due to periodic storage and drainage of stormwater, which might induce structural fatigue on the tunnel lining. Due to complex geological and loading conditions, it is necessary to assess the structural response of the tunnel before construction. Consequently, a series of full-scale loading tests on a single lining ring was conducted on the tunnel lining structure to explore its mechanical behaviors subject to construction and service conditions, i.e., the repeating process of water inflow and drainage was simulated.

3.2. Testing Setup

Figure 7 shows the schematic diagram of the testing setup. The testing system contains an external steel reaction frame, 30 sets of hydraulic ram jacks fixed on the external reaction frame, 15 sets of hydraulic ram jacks positioned on the C-shape beams which are connected with the central column by pulling rods. Two independent systems of hydraulic ram jacks separate the total forces into two backup structures; thus, the required stiffness of the individual frames could be reduced to a large extent. The concentrated forces exerted by the hydraulic ram jacks are transformed to distribution forces through the load-distribution beams connected to the head of hydraulic ram jacks to avoid stress concentration. In order to simulate the increase and decrease of the inner hydraulic head, point loads applied by the two sets of hydraulic jacks are controlled simultaneously during the tests.
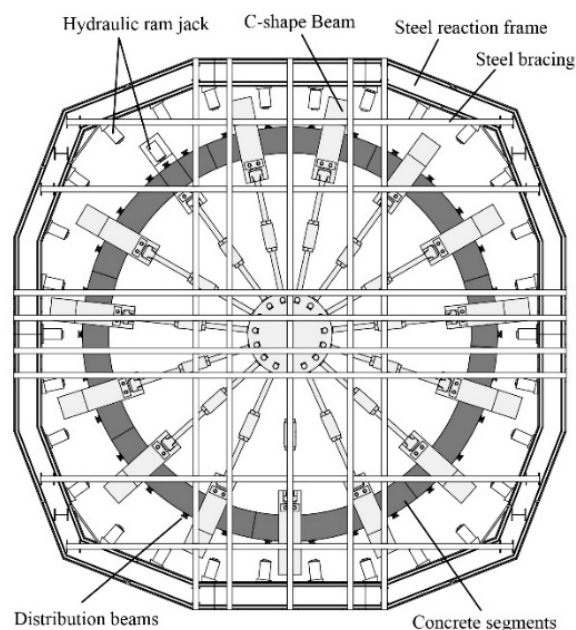

Figure 7. The setup of the loading test (top view).

3.3. Measurement Plan

In order to acquire the deformation of the tunnel lining and validate the current method, two kinds of measurement techniques were implemented, including laser scanning stations and cable displacement transducers (see Figure 8). Note that the laser scanning stations used in the test were Leica P40s, whose scanning accuracy depends on the distance between the laser scanner and the objects to be scanned. The systematic scanning error of the Leica P40 is 3 mm@50 m. Considering that the largest distance from the scanning station to the inner surface of the tunnel lining was around 6 m, the maximum systematic error was approximately 0.36 mm, theoretically.
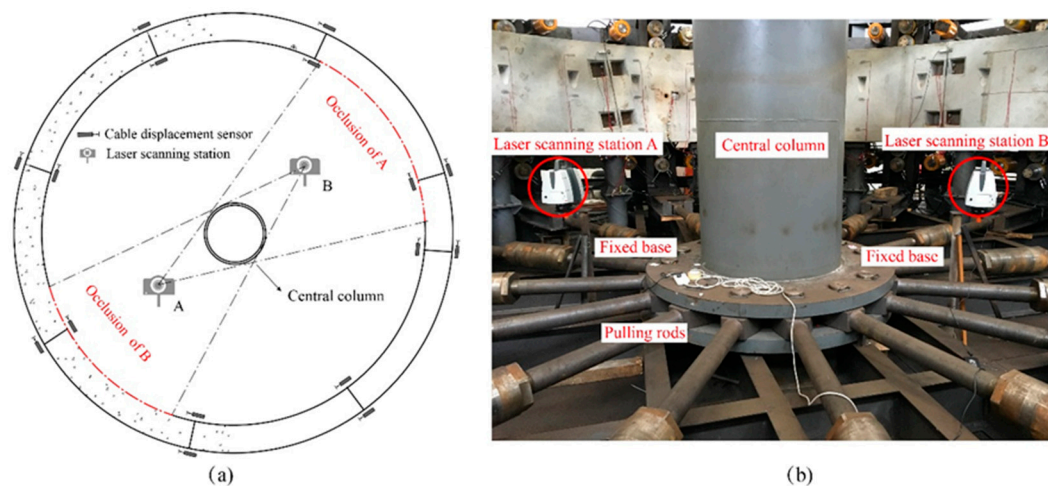
Figure 8. The schematic diagram and picture of the placement of the laser scanning stations: (**a**) schematic diagram (viewed from bottom to top); and (**b**) picture of the site.

Before scanning, two restrictions needed to be specially treated. Firstly, as a self-balanced loading scheme had been designed for the test, a central column was installed in the tunnel center, connected with the external steel frame by pulling rods, and providing counter-forces to balance the testing apparatus (see Figure 8). The existence of the central column made it impossible to install the laser scanning station on the tunnel center, which created occlusions for scanning. Thus, in order to obtain complete point cloud data without any image loss of the segmental tunnel lining, two laser scanning stations that were placed symmetrically aside the central column were used. Therefore, the obstruction of the central column could be overcome as the intact point cloud data could be acquired by merging the data of each station with the aid of 'registration tool' in the Leica Cyclone software. Secondly, during the loading process, excessive vibrations would be induced on the steel frame, which was not favorable for laser scanning. Consequently, fixed bases were installed on the stationary ground to prevent the laser scanning stations from vibration (see Figure 8b).

Since it was dangerous to operate the laser scanning stations by hand as the tunnel lining experienced extremely large loads during the loading tests, the laser scanning stations were controlled by a cell phone through a wireless network. Estimating from the monitored forces of the hydraulic jacks, the scanning process would start when the loads on the segment became stable. The scanning process lasted for one minute, which was fast enough for capturing the deformation of the tunnel lining before it further developed. The point cloud data recorded by the two laser scanning stations could be instantly 'registered' (merged) to obtain the complete raw point cloud data (see Figure 9).
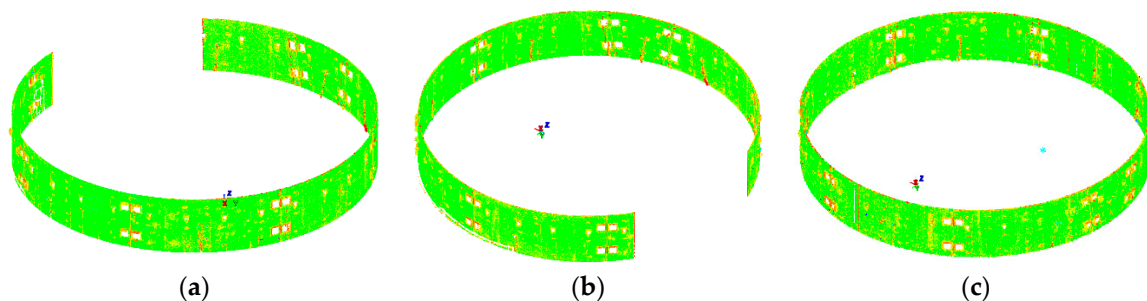

Figure 9. Registration process of the point cloud data from two laser scanning stations: (**a**) point cloud from laser scanning station A; (**b**) point cloud from laser scanning station B; and (**c**) registered full-ring point cloud.

The loading scheme contained two stages: (a) stage I: the external soil-water pressure was gradually increased from burial depth = 0–50 m to simulate the maximum load during construction;

(b) stage II: after the designed burial depth has been reached, the inner hydraulic head was exerted, which was firstly increased from 0–50 m at an interval of 5 m to simulate water inflow and then decreased from 50–0 m at the same interval to simulate drainage. Stage II was repeated for several cycles to simulate the periodic water storage and drainage procedure during the service period. Following the data processing procedures described in Section 2, the deformation could be calculated and visualized shortly after each loading level.

4. Deformation Characteristics of the Water Storage and Sewage Tunnel

4.1. Method Validation

As mentioned before, in order to validate the current method, cable displacement transducers were also installed to measure the convergence deformation (see Figure 8). The results depicted in Figure 10 showed that the maximal vertical convergence deformations at each loading level measured by the two methods were in good agreement with each other. As Figure 10c shows the discrepancies between convergence deformation measured by these two methods were not constant but varied between −4.5% and 4.3%. The mean value of discrepancy for vertical convergence was 0.91% with a standard deviation of 3.54%, and the mean value of discrepancy for horizontal convergence was −1.19% with a standard deviation of 3.21%. The largest observed discrepancy was 4.5%, which confirmed that both the laser scanning technology and the current data processing method were adequately reliable.
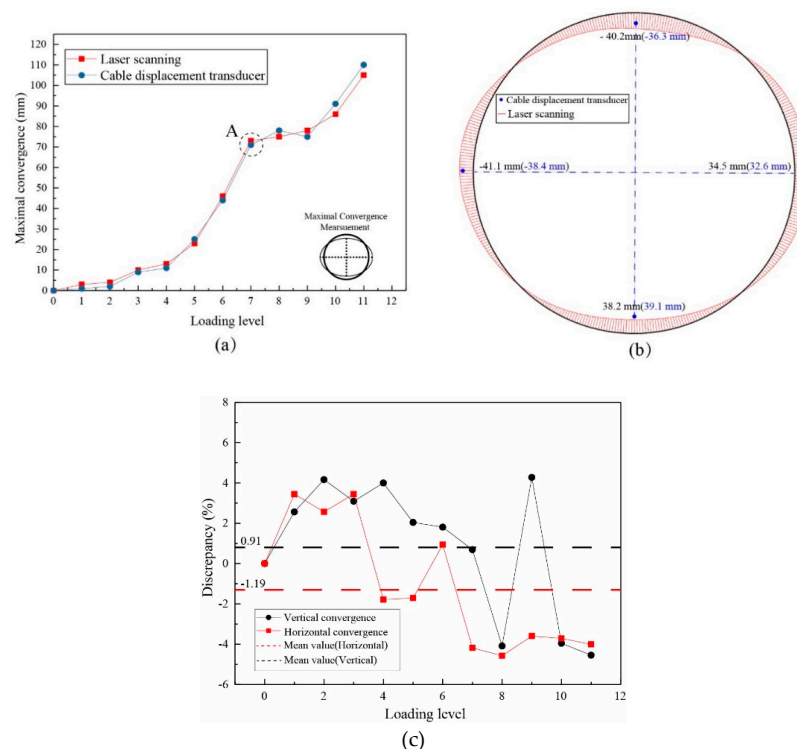

Figure 10. (**a**) Comparison between vertical convergence measured by laser scanning and cable displacement transducer; (**b**) full ring deformation obtained by laser scanning and dispersed deformation obtained by cable displacement transducer at loading stage A (the values in brackets are those measured by cable displacement transducer); and (**c**) the variation of discrepancy at different loading levels.

4.2. Deformation Characteristics of the Testing Tunnel

Figure 11 illustrates the evolution of full-ring deformations at different loading levels, in which the tunnel lining was loaded by firstly increasing the burial depth to 50 m followed by gradually increasing inner hydraulic head to 50 m. The development of tunnel deformation was insignificant

during the stage of increasing burial depth. The largest convergence deformation of 20 mm occurred in the lateral direction when the burial depth reached 50 m. However, an obvious development of the tunnel deformation was observed when the inner hydraulic head was applied to the tunnel lining. The largest convergence deformation increased from 20 mm to 32 mm from an empty state (burial depth = 50 m) to the full-tunnel state (when the tunnel was just full of water). The deformation continued to grow and reached approximately 80 mm when the inner hydraulic head increased further to 50 m. The testing results indicated that the tunnel deformation is more sensitive to the change of inner hydraulic head than to the change of burial depth.
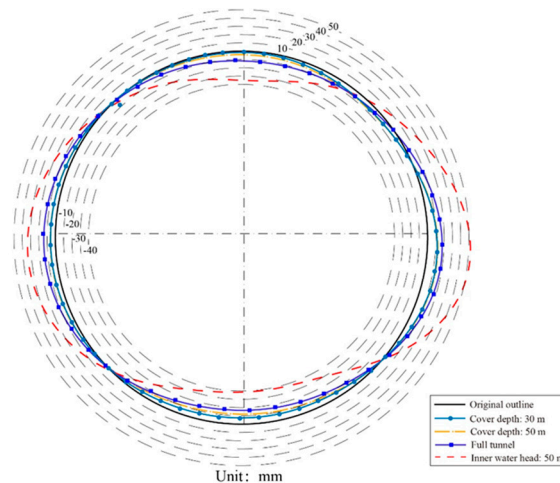

Figure 11. The full-ring deformation contours of the circular tunnel under different loading conditions obtained by TLS.

Figure 12 shows the full-ring horizontal and vertical convergence deformation of the tested stormwater sewage and storage tunnel under cyclic loading. Each cycle incorporated the inflow and discharge of the stormwater with inner hydraulic head varying from 0–50 m. The deformation developed linearly when increasing the burial depth and reached around 20 mm at the designed burial depth (50 m). The deformation continued to grow as the inner hydraulic head was exerted. During the first loading cycle, the deformation grew almost linearly with the increase of the inner hydraulic head but with a steeper slope compared to the deformation evolution curve with increasing burial depth. This may be probably because at the stage of increasing burial depth, both bending moment and axial (normal) force increased and the eccentricity (ratio of bending moment over axial (normal) force) did not increase significantly; whereas, at the stage of increasing inner hydraulic head, the bending moment remained approximately constant but the axial (normal) force dropped rapidly and, thus, the eccentricity increased significantly. Instead of happening at the maximum inner hydraulic head, the largest vertical and horizontal deformation continued to grow at the initial stage of drainage until the hydraulic head has dropped to 20 m. During the subsequent stage of drainage, the deformation decreased nonlinearly with the reduction of inner hydraulic head. Note that in the first loading cycle, compared with the original convergence values, the deformation did not fully recover after the inner hydraulic head has reduced to 0 m. In the subsequent cyclic loading stages, the evolution of both vertical convergence deformation and horizontal expansion deformation with the inner hydraulic head during water inflow and drainage cycles followed a similar trend as the first loading cycle. This 'non-elastic' deformation characteristics of the lining structure may be attributed to the presence of joints whose sliding and dislocation could not fully recover during loading, especially at the stage of varying inner hydraulic head. As Figure 13 shows, the convergence deformations were not stabilized but kept growing as the loading cycle proceeded. Similar observations were reported by Huang et al. [46] in three-ring loading tests for the same project.
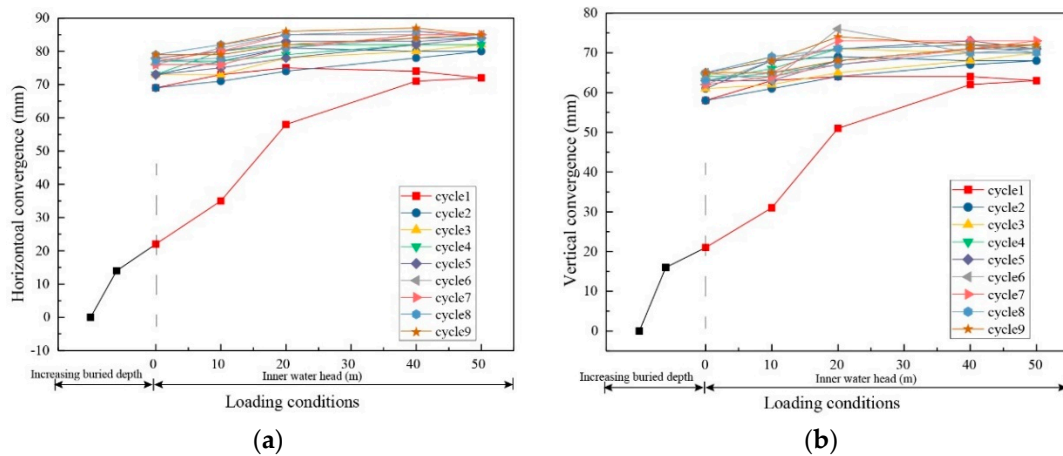
Figure 12. The full-ring convergence deformation of the stormwater sewage and storage tunnel under cyclic loadings: (**a**) horizontal; and (**b**) vertical.
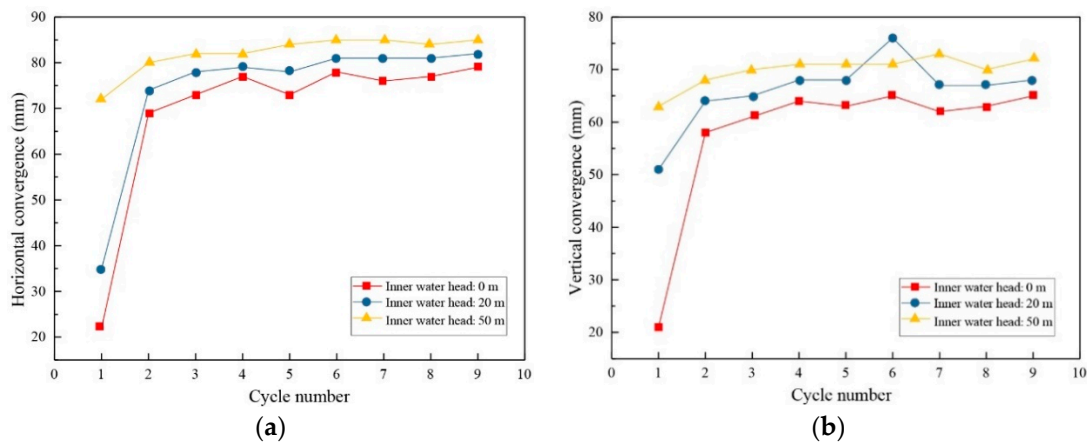

Figure 13. Evolution of convergence deformation at representative loading stages with the number of loading cycles: (**a**) horizontal; and (**b**) vertical.

5. Discussion and Conclusions

In this paper, a new methodology to process and visualize the full-ring deformation during structural loading tests on tunnel lining using the terrestrial laser scanning technique was proposed. Using this method, the two-dimensional full-ring deformation could be extracted from the three-dimensional point cloud data in a prescribed polar coordinate system, which could be obtained and visualized efficiently and accurately with the aid of the developed post-processing software Cloud Viewer. Particular treatment for discontinuities on the tunnel lining caused by hand holes and grooves on the segments was elucidated. The current method was validated by comparing the measured deformation data with that obtained by the cable displacement transducers in the full-scale loading test of a stormwater storage and sewage tunnel beneath the Suzhou River of Shanghai. In addition to the accurate measurement of deformation at cable displacement transducer locations, the proposed method gave the deformed outline of the testing lining and the evolution of the full-ring deformation during the tests. Furthermore, the evolution of the largest convergence deformation under repeating water inflow and drainage loading conditions was captured. It was shown that:

(1) The deformation of lining segment is more sensitive to the change of inner hydraulic head than that of burial depth as the eccentricity was larger and grew more rapidly in the former situation than in the latter situation

(2) The deformation could not fully recover after the inner hydraulic head has been reduced to 0 m due to the presence of joints, and the vertical and horizontal convergence at each

hydraulic head level continued to grow as the loading cycle proceeded. This observation is of practical significance as the deformation was not stabilized but kept growing during water-inflow-and-drainage cycles, which when reaching some limiting point may induce the fatigue failure of the entire lining structure. This risk should be considered when designing the lining structure.

There are also some limitations of using TLS technology and the current data processing method. Firstly, the cost of using the laser scanning station is much higher than the traditional cable displacement transducers, making it uneconomical for small-scale experiments. Secondly, the preliminary elimination of the noise points as described in Section 3 needs to be done manually, which would be time-consuming especially when a large quantity of point cloud data requires processing. Finally, the current processing method adopts the curve-fitting method to obtain the deformation contour based on the representative points (See Section 2.2.2), thus the dislocation between the segments could not be gained. Consequently, in order to measure the dislocation, traditional measurements such as the displacement transducers must be used at the joints in the loading tests. Considering these limitations, future efforts will be devoted to improving the automation of the data processing procedures and the current data processing method, which would enable analysis of the dislocation between segments.

Despite these deficiencies, the current work provides a promising solution for automatic monitoring and analysis of tunnel deformation. The data processing and visualization techniques developed in the current study may be extended to in situ monitoring of operation tunnels' deformation, which will be useful for maintenance and life-cycle analysis.

Author Contributions: Z.Z. organized the entire paper and is responsible for the data processing algorithm. T.Y. wrote most parts of the paper and did some data analyses. X.H. contributed partially to the data processing algorithm, and was in charge of the full-scale loading tests and did the final editing of the paper. F.Z. implemented the visualization algorithm and developed theCloud Viewer software. Y.Z. and W.L. participated in the full-scale loading tests and did the preliminary data processing.

Conflicts of Interest: None.

References

1. Liu, X.; Jiang, Z.J.; Yuan, Y.; Mang, H.A. Experimental investigation of the ultimate bearing capacity of deformed segmental tunnel linings strengthened by epoxy-bonded steel plates. *Struct. Infrastruct. Eng.* **2017**, *14*, 685–700. [CrossRef]
2. Liu, X.; Liu, Z.; Ye, Y.H.; Bai, Y.; Zhu, Y.H. Mechanical behavior of quasi-rectangular segmental tunnel linings: Further insights from full-scale ring tests. *Tunn. Undergr. Space Technol.* **2018**, *79*, 304–318. [CrossRef]
3. Zhu, Y.; Zhang, Z.X.; Huang, X.; Zhang, G. Prototype loading tests on full-ring segmental lining of rectangular shield tunnel. *J. Shanghai Jiaotong Univ.* **2018**, *23*, 746–757. [CrossRef]
4. Nuttens, T.; Stal, C.; Backer, H.D.; Schotte, K.; Van Bogart, P.; Wulf, A.D. Methodology for the ovalization monitoring of newly built circular train tunnels based on laser scanning: Liefkenshoek Rail Link (Belgium). *Autom. Constr.* **2014**, *43*, 1–9. [CrossRef]
5. Schueremans, L.; Van Genechten, B. The use of 3D-laser scanning in assessing the safety of masonry vaults—A case study on the church of Saint-Jacobs. *Opt. Lasers Eng.* **2009**, *63*, 142–154. [CrossRef]
6. Clarke, T.A.; Lindsey, N.E. Profiling methods reviewed. *Tunn. Tunn. Inter.* **1992**, *24*, 29–31.
7. Wang, W.X.; Zhao, W.S.; Huang, L.X.; Vimarlund, V.; Wang, Z.W. Applications of terrestrial laser scanning for tunnels: a review. *J. Traffic Transp. Eng. (English Edition)* **2014**, *1*, 325–337. [CrossRef]
8. Fekete, S.; Diederichs, M.; Lato, M. Geotechnical and operational applications for 3-dimensional laser scanning in drill and blast tunnels. *Tunn. Undergr. Space Technol.* **2010**, *25*, 614–628. [CrossRef]

9. Lague, D.; Brodu, N.; Leroux, J. Accurate 3D comparison of complex topography with terrestrial laser scanner: Application to the Rangitikei canyon (N-Z). *ISPRS J. Photogramm. Remote Sens.* **2013**, *82*, 10–26. [CrossRef]

10. Abellan, A.; Jaboyedoff, M.; Oppikofer, T.; Vilaplana, J.M. Detection of millimetric deformation using a terrestrial laser scanner: experiment and application to a rock fall event. *Nat. Hazards Earth Syst. Sci.* **2009**, *9*, 365–372. [CrossRef]

11. Aguilar, F.J.; Aguilar, M.A.; Carvaj, F. Effects of terrain morphology, sampling density, and interpolation methods on grid DEM accuracy. *Photogramm. Eng. Remote Sens.* **2005**, *71*, 805–816. [CrossRef]

12. Jung, J.; Hong, S.; Yoon, S.; Kim, J.; Heo, J. Automated 3D wireframe modeling of indoor structures from point clouds using constrained least-squares adjustment for as-built BIM. *J. Comput. Civ. Eng.* **2016**, *30*, 04015074. [CrossRef]

13. Dimitrov, A.; Golparvar-Fard, M. Robust NURBS surface fitting from unorganized 3D point clouds for infrastructure as-built modeling. In Proceedings of the International Conference on Computing in Civil and Building Engineering, Orlando, FL, USA, 23–25 June 2014; pp. 81–88.

14. Dimitrov, A.; Golparvar-Fard, M. Segmentation of building point cloud models including detailed architectural/structural features and MEP systems. *Autom. Constr.* **2015**, *51*, 32–45. [CrossRef]

15. Guan, H.; Li, J.; Yu, Y.; Wang, C.; Chapman, M.; Yang, B. Using mobile laser scanning data for automated extraction of road markings. *ISPRS J. Photogramm. Remote Sens.* **2014**, *87*, 93–107. [CrossRef]

16. Smadja, L.; Ninot, J.; Gavrilovic, T. Road extraction and environment interpretation from lidar sensors. *Int. Arch. Photogramm. Remote Sens. Spat. Inf. Sci.* **2010**, *38*, 281–286.

17. Toth, C.; Paska, E.; Brzezinska, D. Using road pavement markings as good control for lidar data. *Int. Arch. Photogramm. Remote Sens. Spat. Inf. Sci.* **2008**, *37*, 189–196.

18. O'Neal, M.A.; Pizzuto, J.E. The rates and spatial patterns of annual riverbank erosion revealed through terrestrial laser-scanner surveys of the South River, Virginia. *Earth Surf. Process. Landf.* **2011**, *36*, 695–701. [CrossRef]

19. Resop, J.P.; Hession, W.C. Terrestrial laser scanning for monitoring streambank retreat: a comparison with traditional surveying techniques. *J. Hydraul. Eng.* **2010**, *136*, 794–798. [CrossRef]

20. Milan, D.J.; Heritage, G.L.; Hetherington, D. Application of a 3D laser scanner in the assessment of erosion and deposition volumes and channel change in a proglacial river. *Earth Surf. Process. Landf.* **2007**, *32*, 1657–1674. [CrossRef]

21. Lee, J.; Son, H.; Kim, C.; Kim, C. Skeleton-based 3D reconstruction of as-built pipelines from laser-scan data. *Autom. Constr.* **2013**, *35*, 199–207. [CrossRef]

22. Kawashima, K.; Kanai, S.; Date, H. Automatic recognition of piping system from large-scale terrestrial laser scanned point cloud. *J. Jpn. Soc. Precis. Eng.* **2012**, *78*, 722–729. [CrossRef]

23. Barbarella, M.; Fiani, M. Monitoring of large landslides by terrestrial laser scanning techniques: Field data collection and processing. *Eur. J. Remote Sens.* **2013**, *46*, 126–151. [CrossRef]

24. Barbarella, M.; Fiani, M.; Lugli, A. Landslide monitoring using multitemporal terrestrial laser scanning for ground displacement analysis. *Geomat. Nat. Hazards Risk* **2013**, *6*, 398–418. [CrossRef]

25. Derron, M.H.; Jaboyedoff, M. LIDAR and DEM techniques for landslides monitoring and characterization. *Nat. Hazards Earth Syst. Sci.* **2010**, *10*, 1877–1879. [CrossRef]

26. Cacciari, P.P.; Futai, M.M. Mapping and characterization of rock discontinuities in a tunnel using 3D terrestrial laser scanning. *Bull. Eng. Geol. Environ.* **2016**, *75*, 223–237. [CrossRef]

27. Cacciari, P.P.; Futai, M.M. Modeling a shallow rock tunnel using terrestrial laser scanning and discrete fracture networks. *Rock Mech. Rock Eng.* **2017**, *50*, 1217–1242. [CrossRef]

28. Fekete, S.; Diederichs, M. Integration of three-dimensional laser scanning with discontinuum modelling for stability analysis of tunnels in blocky rockmasses. *Int. J. Rock Mech. Min. Sci.* **2013**, *57*, 11–23. [CrossRef]

29. Lato, M.; Diederichs, M.S.; Hutchinson, D.J.; Harrap, R. Optimization of LiDAR scanning and processing for automated structural evaluation of discontinuities in rockmasses. *Int. J. Rock Mech. Min. Sci.* **2009**, *46*, 194–199. [CrossRef]

30. Charbonnier, P.; Chavant, P.; Foucher, P.; Muzet, V.; Prybyla, D.; Perrin, T.; Grussenmeyer, P.; Guillemin, S. Accuracy assessment of a canal-tunnel 3D model by comparing photogrammetry and laser scanning recording techniques. *Int. Arch. Photogramm. Remote Sens. Spat. Inf. Sci.* **2013**, *40*, 171–176. [CrossRef]

31. Gikas, V. Three-dimensional laser scanning for geometry documentation and construction management of highway tunnels during excavation. *Sensors* **2012**, *12*, 11249–11270. [CrossRef] [PubMed]

32. Tsakiri, M.; Lichti, D.; Pfifer, N. Terrestrial laser scanning for deformation monitoring. In Proceedings of the 3rd IAG Symposium on Geodesy for Geotechnical and Structural Engineering and 12th FIG Symposium on Deformation Measurement, Baden, Austria, 22–24 May 2006.

33. Pejić, M. Design and optimisation of laser scanning for tunnels geometry inspection. *Tunn. Undergr. Space Technol.* **2013**, *37*, 199–206. [CrossRef]

34. Yoon, S.K.; Sagong, M.; Lee, J.S.; Lee, K.S. Feature extraction of a concrete tunnel liner from 3D laser scanning data. *NDT&E Int.* **2009**, *42*, 97–105.

35. Han, S.; Cho, H.; Kim, S.; Jung, J.; Heo, J. Automated and Efficient Method for Extraction of Tunnel Cross Sections Using Terrestrial Laser Scanned Data. *J. Comput. Civ. Eng.* **2013**, *27*, 274–281. [CrossRef]

36. Cheng, Y.; Qiu, W.; Lei, J. Automatic Extraction of Tunnel Lining Cross-Sections from Terrestrial Laser Scanning Point Clouds. *Sensors* **2016**, *16*, 1648. [CrossRef] [PubMed]

37. Walton, G.; Delaloye, D.; Diederichs, M.S. Development of an elliptical fitting algorithm to improve change detection capabilities with applications for deformation monitoring in circular tunnels and shafts. *Tunn. Undergr. Space Technol.* **2014**, *43*, 336–349. [CrossRef]

38. Kang, Z.; Zhang, L.; Tuo, L.; Wang, B.; Chen, J. Continuous Extraction of Subway Tunnel Cross Sections Based on Terrestrial Point Clouds. *Remote Sens.* **2014**, *6*, 857–879. [CrossRef]

39. Tan, K.; Cheng, X.; Ju, Q. Combining mobile terrestrial laser scanning geometric and radiometric data to eliminate accessories in circular metro tunnels. *J. Appl. Remote Sens.* **2016**, *10*, 030503. [CrossRef]

40. Xie, X.; Lu, X. Development of a 3D modeling algorithm for tunnel deformation monitoring based on terrestrial laser scanning. *Undergr. Space* **2017**, *2*, 16–29. [CrossRef]

41. Cao, Z.; Chen, D.; Shi, Y.; Zhang, Z.; Jin, F.; Yun, T.; Xu, S.; Kang, Z.; Zhang, L. A flexible architecture for extracting metro tunnel cross sections from terrestrial laser scanning point clouds. *Remote Sens.* **2019**, *11*, 297. [CrossRef]

42. Araki, T.; Yoshida, H. Optical distance meter using a pulsed laser diode and fast avalanche photo diode for measurements of molten steel levels. *J. Dyn. Syst. Meas. Control* **1996**, *188*, 800–803. [CrossRef]

43. Nissinen, I.; Kostamovaara, J. On-Chip voltage reference-based time-to-digital converter for pulsed time-of-flight laser radar measurements. *IEEE Trans. Instrum. Meas.* **2009**, *58*, 1938–1948. [CrossRef]

44. LeicaGeosystems. Leica Cyclone 3D Point Cloud Processing Software. 2011. Available online: http://hds.leica-geosystems.com/en/Leica-Cyclone_6515.htm (accessed on 20 July 2017).

45. Huang, X.; Zhu, Y.T.; Zhang, Z.X.; Zhu, Y.F.; Wang, S.F.; Zhuang, Q.W. Mechanical behaviour of segmental lining of a sub-rectangular shield tunnel under self-weight. *Tunn. Undergr. Space Technol.* **2018**, *74*, 131–144. [CrossRef]

46. Huang, X.; Liu, W.; Zhang, Z.X.; Wang, Q.; Wang, S.F.; Zhuang, Q.W.; Zhu, Y.T.; Zhang, C. Exploring the three-dimensional response of a water storage and sewage tunnel based on full-scale loading tests. *Tunn. Undergr. Space Technol.* **2019**, *88*, 156–168. [CrossRef]